

# The Influence of Physical Properties of ZnO Films on the Efficiency of Planar ZnO/Perovskite/P3HT Solar Cell

Zhiwen Qiu, Shuai Yuan, Haibo Gong, Hailiang Zhang, Xiaofeng Qiu, Ting Luo, and Bingqiang Cao<sup>†</sup>

Materials Research Center for Energy and Photoelectrochemical Conversion, School of Material Science and Engineering, University of Jinan, Jinan 250022, Shandong, China

ZnO thin films prepared by pulsed laser deposition at low temperature are utilized as the electron transport layer in  $\text{CH}_3\text{NH}_3\text{PbI}_{3-x}\text{Cl}_x$ -based perovskite solar cells with a planar heterojunction structure. Oxygen pressure greatly influences the transparent and conductive properties of ZnO films, which are extremely important as electron transport layer for the perovskite solar cells. The transparent and conductive properties of the films under different oxygen pressures are studied by ultraviolet-visible spectrophotometer and Hall effect measurement system. Through controlling the oxygen pressure, transparent ZnO films with high conductivity are grown and adopted as electron transport layer for planar perovskite solar cell with a power conversion efficiency of 6.3%. After further surface modification of ZnO electron transport layer with [6,6]-phenyl-C61-butyric acid methyl ester, the efficiency of the planar solar cell increases to 7.5%.

**Keywords:** zinc oxide; pulsed laser deposition; oxygen pressure; perovskite solar cell; electron transport layer

## I. Introduction

SINCE organometal halide perovskite sensitized solar cells ( $\text{CH}_3\text{NH}_3\text{PbX}_3$ , X: Cl, Br, or I) were firstly reported by Miyasaka et al.,<sup>1</sup> a major scientific breakthrough in the field of photovoltaics has been the emergence of organometal perovskites as absorber materials, achieving exceptional progress in solar cell performance.<sup>2</sup> Typically,  $\text{CH}_3\text{NH}_3\text{PbI}_3$  has a direct optical band gap of around 1.5 eV,<sup>3</sup> low exciton binding energy (~45 meV),<sup>4</sup> and apparent tolerance of structural defects, high optical absorption, and long charge carrier diffusion lengths.<sup>5</sup> So far, the most efficient perovskite solar cells with PCE over 15% have a typical planar P–i–N structure of HTL/perovskite/ETL. HTL represents the *p*-type hole transport layer, and ETL represents the *n*-type electron transport layer.<sup>6–8</sup> The ETL and HTL layers not only collect the currents but also block the holes and the electrons, respectively. They also prevent the perovskite active layer from the direct contact with electrodes to reduce recombination of photocurrent.<sup>9</sup> The film roughness of electron transport layer also influences the growth of perovskite layer, especially for its surface morphology. Moreover, the electrical and optical properties of ETLs can significantly affect the performance of perovskite solar cells in terms of fill factor (FF), open-circuit voltage ( $V_{oc}$ ), and short-circuit current ( $J_{sc}$ ). So, selecting ETL with controlled property is essential to understand the solar cell photovoltaic processes such as photocarrier separation, transport, extraction, and recombination.<sup>10</sup>

In a planar P–i–N perovskite solar cell, a metal oxide dense film, such as  $\text{TiO}_2$ <sup>11,12</sup> or  $\text{ZnO}$ <sup>13,14</sup> is usually used as an electron transport layer to beneficially transfer the electrons and block the holes. Although the highest efficiency was obtained with  $\text{TiO}_2$  film-based perovskite solar cells,<sup>15</sup> ZnO is also very attractive owing to the following material characteristics. First, ZnO is a wide band semiconductor with similar band gap structure to that of  $\text{TiO}_2$  but has higher electron mobility.<sup>16–18</sup> Importantly, high crystalline ZnO films can be grown at low temperature without sintering processes.<sup>19</sup> Several growth methods including sol–gel process, electrodeposition, and sputtering could be adopted for ZnO films.<sup>20</sup> For example, Park *et al.*<sup>21</sup> prepared ZnO nanorod-based perovskite solar cell in the absence of a compact  $\text{TiO}_2$  blocking layer with a power conversion efficiency (PCE) of 11.13%. However, high processing temperature (450°C) was adopted to anneal the ZnO nanorods. Kelly et al.<sup>22</sup> reported the use of ZnO nanoparticles thin film as ETL in a  $\text{CH}_3\text{NH}_3\text{PbI}_3$ -based solar cell without high-temperature sintering. But impurities can be easily introduced into ZnO nanoparticles by a solution method. Mahmood et al.<sup>23</sup> explored a double-layered ZnO film for mesoscopic perovskite thin film solar cell, showing PCE of 10.35%. The low-temperature grown ZnO film as electron transport layer in perovskite solar cells highlight the opportunities to further improve the efficiency by optimizing the ETL optical and electrical properties. For example, Song *et al.*<sup>24</sup> adopted spin-coated ZnO thin film as electron transport layer and the layer thickness as a key parameter for the photovoltaic performance was optimized. Moreover, precise controlling the semiconductor property of ETL like its transparency and conductivity is very important for perovskite solar cells, yet there is a dearth of effort in this area. Only few reports discussed the effects of the nonstoichiometry defects of the metal oxide electron transport layer on the photovoltaic performance of the planar perovskite solar cell.<sup>25</sup> Therefore, we need to explore new method to grow electron transport layer in a controlled manner, and regulate their physical property.

Pulsed laser deposition (PLD) is now one of the most successful growth techniques to obtain high-quality oxide thin films and nanostructures.<sup>26–28</sup> In addition, although undoped ZnO is a typical *n*-type semiconductor, the growth environment, such as oxygen partial pressure, can greatly influence the transparent and conductive properties of ZnO film. In this regard, Garcia *et al.*<sup>29</sup> stated that the resistivity of polycrystalline undoped ZnO films can be changed by more than 10 orders of magnitude by controlling the oxygen partial pressure with rf-magnetron sputtering. Further, it was also reported that the oxygen vacancy can increase the carrier density of ZnO film, which also possibly influenced its electronic structure.<sup>30</sup> These properties were both important ETL characteristics for the perovskite solar cells.

Herein, we studied systematically the effect of different oxygen pressures on the semiconducting properties of ZnO thin films grown by PLD, which showed great influence on the photovoltaic efficiency of the  $\text{CH}_3\text{NH}_3\text{PbI}_{3-x}\text{Cl}_x$ -based

H. Du—contributing editor

Manuscript No. 38525. Received April 28, 2016; approved August 8, 2016.

<sup>†</sup>Author to whom correspondence should be addressed. e-mail: mse\_caobq@ujn.edu.cn

perovskite solar cells when ZnO film was used as ETL. Such ZnO layer was substantially thinner and required no high-temperature sintering in contrast to the mesoporous TiO<sub>2</sub> film. Moreover, as PLD growth technique had the advantages such as the short growth cycle, less impurity, and better crystallinity, we can adjust the physical properties of ZnO ETL by controlling the growth condition like oxygen pressures. The optimized growth conditions for ZnO ETL were obtained for ZnO/CH<sub>3</sub>NH<sub>3</sub>PbI<sub>3-x</sub>Cl<sub>x</sub>/P3HT/Au planar solar cell with an efficiency of 6.3%. After further surface modification of ZnO ETL with a PCBM layer, the efficiency increased to 7.5%. These characteristics favored the development of large area flexible solar cells with a pre-designed process.

## II. Experimental Procedure

### (1) Growth of ZnO Thin Films Under Different Oxygen Pressures

ZnO targets made from pressed and sintered oxide powders were adopted for PLD. KrF excimer laser (CompexPro 205, Coherent) pulses with a 10 Hz repetition frequency were applied. Fluorine-doped tin oxide (FTO)-coated glass (15 Ω/sq, Pilkington, Minato-ku, Tokyo, Japan) was used as substrate for ZnO film growth at ambient temperature. The O<sub>2</sub> pressure was controlled in the range of 10<sup>-3</sup> Pa–10<sup>2</sup> Pa. The laser energy density focused on the target was about 2 J/cm<sup>2</sup>. The distance between target and substrate was 100 mm.

### (2) Fabrication of CH<sub>3</sub>NH<sub>3</sub>PbI<sub>3-x</sub>Cl<sub>x</sub> Perovskite Solar Cells

Perovskite solar cells were prepared as schematically shown in Fig. 1. The devices were fabricated with the structure of FTO/ZnO/CH<sub>3</sub>NH<sub>3</sub>PbI<sub>3-x</sub>Cl<sub>x</sub>/P3HT/Au. A 70 nm ZnO layer was prepared by PLD method under different oxygen pressures. We used a mixture of PbCl<sub>2</sub> and PbI<sub>2</sub> as the precursor, and spin-coated at 5000 rpm on the compact ZnO film. Then, it was annealed at 70°C for 30 min. The CH<sub>3</sub>NH<sub>3</sub>I solution was added onto the surface and kept for 46 s and spin-coated at 5000 rpm for 30 s to form the CH<sub>3</sub>NH<sub>3</sub>PbI<sub>3-x</sub>Cl<sub>x</sub> film. The film color changed from chartreuse to dark brown, indicating the formation of the perovskite. Then, P3HT was coated onto the perovskite layer at 2500 rpm for 30 s. Finally, Au electrodes were thermally deposited under high vacuum through a shadow mask. The

devices with PCBM as modified layer were fabricated on the basis of the structure of FTO/ZnO/PCBM/CH<sub>3</sub>NH<sub>3</sub>PbI<sub>3-x</sub>Cl<sub>x</sub>/P3HT/Au. PCBM film was cast from a solution with 20 mg/mL in chlorobenzene at 3500 rpm for 30 s. Sample and device characterization details were presented as Supporting Information.

## III. Results and Discussions

### (1) Effect of Oxygen Pressure on ZnO Transparent and Conductive Properties

When ZnO film is used as ETL, the first physical property to be checked is the optical transmittance. Figure 2 shows the typical optical photos and according transmission spectra of the ZnO films grown under different oxygen pressures, from 10<sup>-3</sup> Pa to 10<sup>2</sup> Pa. ZnO thin film is black when the oxygen pressure is under 10<sup>-3</sup> Pa, which is due to the incomplete oxidation of Zn<sup>2+</sup> ions produced by laser ablation. ZnO film under 2 Pa shows a slight yellow color. With the oxygen pressure increasing, the color is lighter and the film becomes transparent gradually. But when the oxygen pressure reaches 10<sup>2</sup> Pa, the film becomes opaque due to the surface roughness. The UV/vis transmittance spectra of the ZnO samples prepared under different oxygen pressures are also shown in Fig. 2. The transmittance of the sample under 10<sup>-3</sup> Pa is only 30% in the visible wavelength range. With the increase of oxygen pressures in the range of 3 × 10<sup>-2</sup> Pa–30 Pa, the transmittance of the samples become higher. Typically, all the films in the range of 2–20 Pa exhibit typical transmittance higher than 90%. But when oxygen pressure reaches 100 Pa, the crystal quality of the film reduces and a large number of particles appear on the surface. The film becomes opaque and the optical transmittance of this film suddenly drops to 20%. When ZnO film acts as ETL of the perovskite solar cell, the high optical transmittance is beneficial to improve the utilization efficiency of solar radiation. According to the transparent properties of the ZnO films, we choose the ZnO film grown under oxygen pressure of 2–20 Pa.

Resistivity (ρ) is the second physical property should be considered when ZnO film is used as ETL, which is closely related with the PLD growth conditions. Figure 3(a) shows an X-ray photoelectron survey spectrum (XPS) of ZnO film prepared under 10<sup>-1</sup> Pa. In Fig. 3(b), the peaks at 1043.49 and 1020.37 eV correspond to the bonding energies (BE) of Zn2p<sub>1/2</sub> and Zn2p<sub>3/2</sub>, respectively, which are attributed to Zn–O bonds.<sup>31</sup> Figures 3(c)–(e) are XPS spectra of O1s

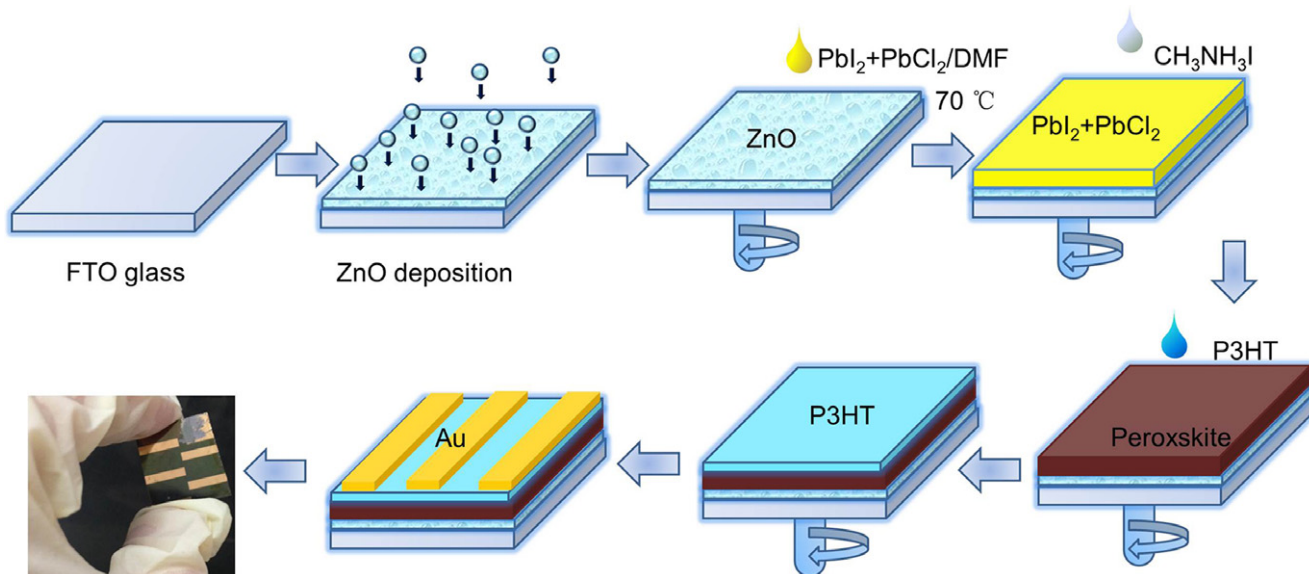


Fig. 1. Schematic illustration of perovskite solar cells fabricated by two-step sequential deposition method.

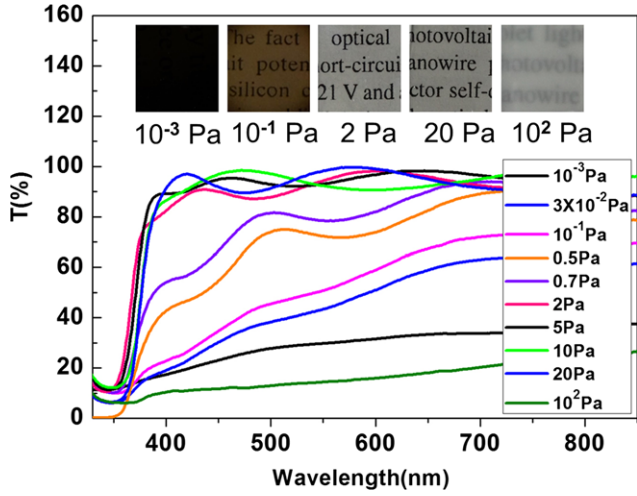


Fig. 2. The photos of ZnO films and transmittance spectra of ZnO films prepared under different oxygen pressures ( $10^{-3}$  Pa– $10^2$  Pa).

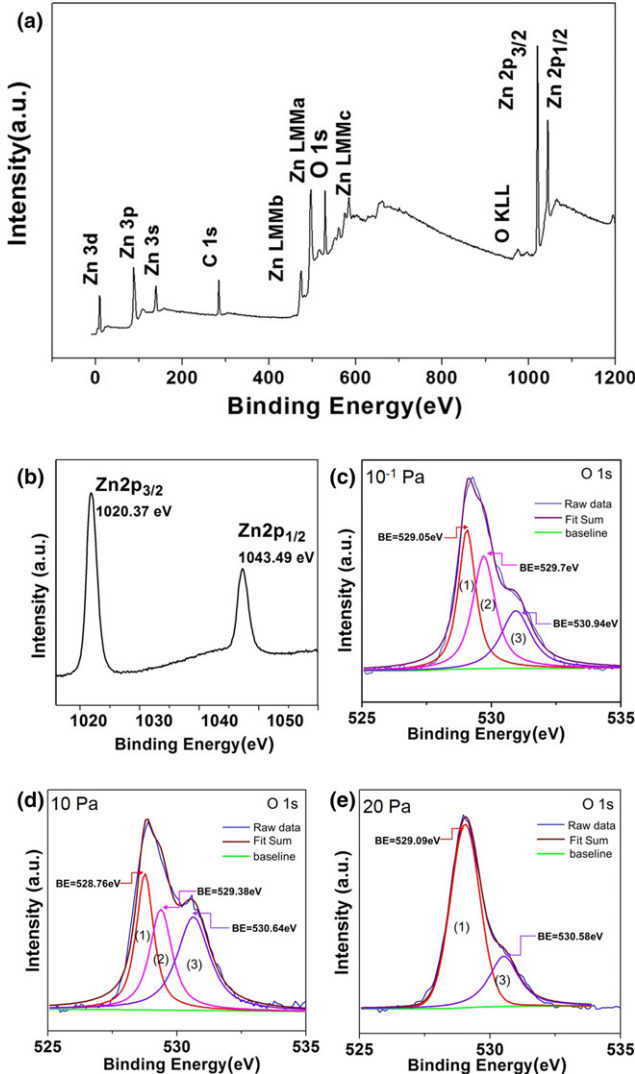


Fig. 3. (a) X-ray photoelectron survey spectrum of ZnO film prepared under  $10^{-1}$  Pa, (b) high-resolution X-ray photoelectron spectra of Zn $2p$  of ZnO film prepared under  $10^{-1}$  Pa, XPS spectra of O  $1s$  of ZnO films under different oxygen pressures (c)  $10^{-1}$  Pa, (d) 10 Pa, and (e) 20 Pa.

detected from ZnO films grown under different oxygen pressures. Only Zn, O, and C elements are detected, which indicates that there is no impurity in the PLD-grown ZnO film.<sup>32</sup> But, the Zn/O ratio is different when the oxygen growth pressure changes, as shown in Table I. At low oxygen growth pressure of  $10^{-1}$  Pa, due to the formation of oxygen vacancy ( $V_o$ ) defects, the Zn/O ratio is 1.11. This can be proved by the O $1s$  peak analysis. Generally, the O $1s$  core-level spectrum of ZnO shows three different peaks. The Gaussian-fitted peaks marked as (1), (2), and (3) from the low BE to high BE are shown in Figures 3(c)–(e). Peak (1) is assigned to O $^{2-}$  ions in the Zn–O bonding of the wurtzite ZnO.<sup>31</sup> Peak (2) is associated with O $^{2-}$  ions in the oxygen-deficient regions within the matrix of ZnO.<sup>33</sup> Peak (3) is usually due to the presence of loosely bound oxygen on the surface of ZnO films, e.g., O $_2$ .<sup>17</sup> The detailed composition analysis of O $1s$  peak was shown in Table S1 in Supporting Information. For ZnO film of  $10^{-1}$  Pa, a clear peak (2) from oxygen vacancy ( $V_o$ ) defects was observed together with the relative weak peak (3) from bound oxygen. When the oxygen pressure increases to 10 Pa, the Zn/O ratio decreases to 0.78 as a result of decreasing  $V_o$  defects and increasing O $_2$ . When the oxygen pressure increases to 20 Pa, the Zn/O ratio increases to 0.87. In this case, peak (2) due to  $V_o$  disappear and peak (3) also decrease. In summary, the Zn/O ratio first decreases and then increases with a turning point at growth pressure of 10 Pa.

Oxygen vacancy is one of the most important defects that affect the electrical behavior of ZnO film,<sup>34</sup> and the above XPS analysis can support well the Hall data shown in Fig. 4, where the resistivity ( $\rho$ ), carrier concentration ( $n$ ), and carrier mobility ( $\mu$ ) of ZnO films are plotted as a function of oxygen pressure. As  $V_o$  indicated with peak (2) is the main n-type donor for ZnO film, the electron concentration continues to decrease from  $2.2 \times 10^{19}$ – $7.5 \times 10^{16}$  cm $^{-3}$  when the oxygen pressures increase from  $10^{-1}$  Pa to 20 Pa. The Hall mobility exhibits a similar turning point at 10 Pa. The first mobility decreasing is due to the increasing of adsorbed oxygen that can capture electrons, increase the grain barrier height, and scatter electrons.<sup>35,36</sup> When continuing to increase oxygen

Table I. Summary of Zn/O Ratio of ZnO Films Prepared Under Different Oxygen Pressures

	Zn At. (%)	O At. (%)	Zn/O ratio
0.1 Pa	52.19	47.81	1.11
10 Pa	44.39	55.61	0.78
20 Pa	46.37	53.63	0.87

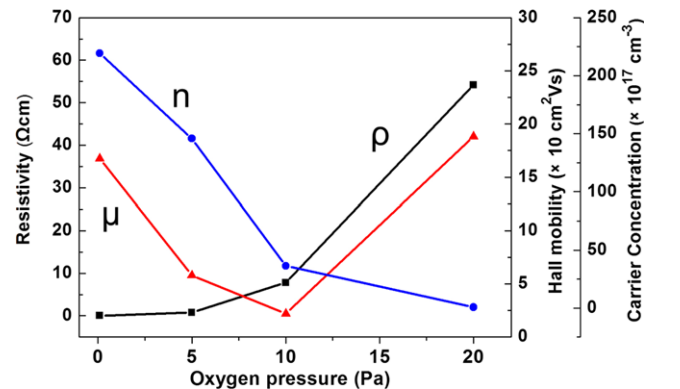
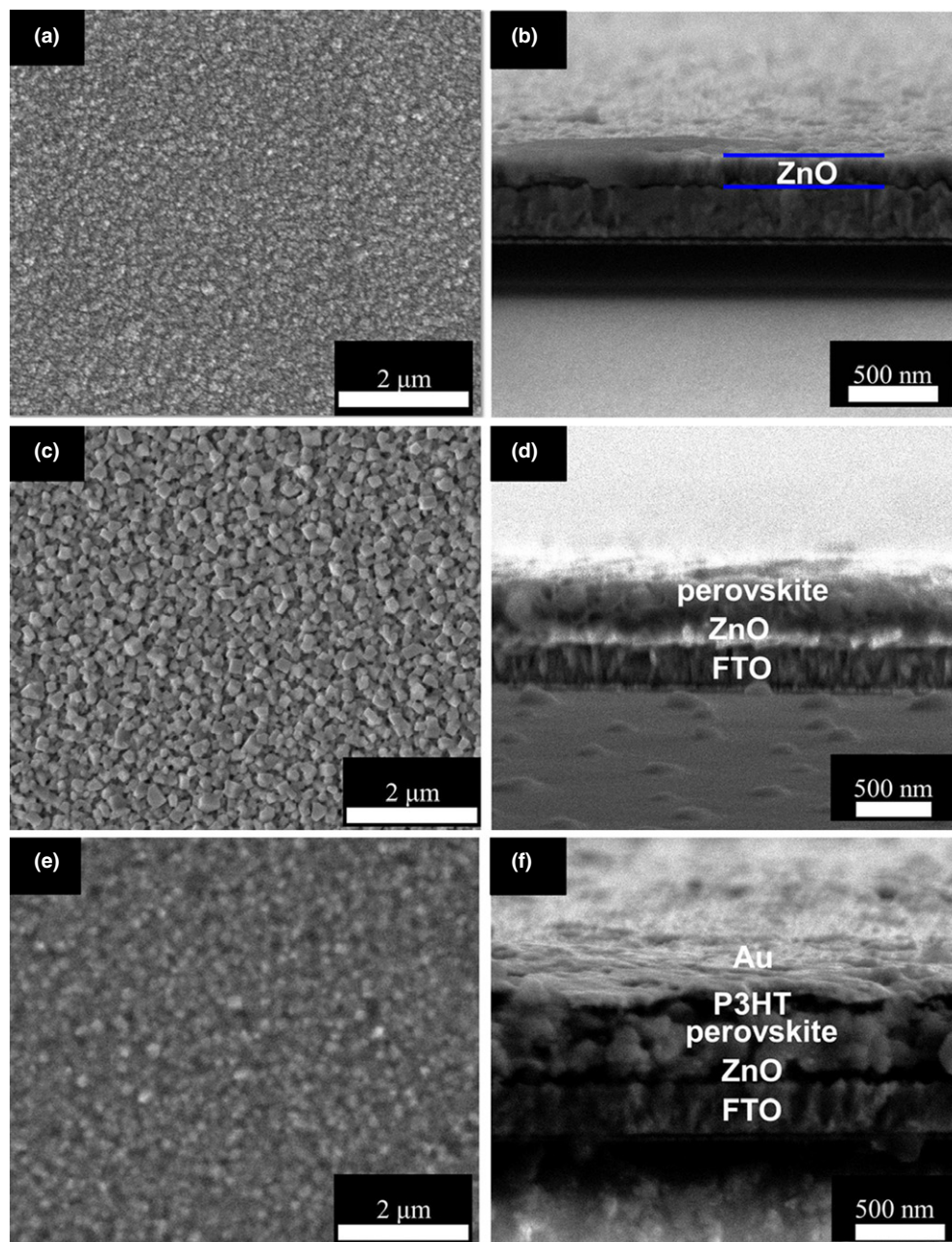


Fig. 4. Resistivity, carrier concentration, and carrier mobility of ZnO thin films as a function of oxygen pressure,  $\rho$  represent the resistivity,  $n$  represent carrier concentration,  $\mu$  represent hall mobility.



**Fig. 5.** Surface cross-sectional scanning electron microscopy images of every layer of the device. (a)–(b) surface (left) and cross-sectional (right) SEM images of ZnO layer, (c)–(d) surface (left) and cross-sectional (right) SEM images of ZnO/CH<sub>3</sub>NH<sub>3</sub>PbI<sub>3-x</sub>Cl<sub>x</sub>, (e) surface SEM image of P3HT layer, (f) cross-sectional SEM image of the device.

pressure (>10 Pa), the amount of adsorbed oxygen decreases. The following Hall mobility increase is due to the decrease of the carrier concentration.<sup>37</sup> The film resistivity is determined by both  $n$  and  $\mu$  with  $\rho = (nq\mu)^{-1}$ , where  $q$  is the elementary charge. The films resistivity increases from  $1.7 \times 10^{-3} \Omega\text{-cm}$  to  $54 \Omega\text{-cm}$  from  $10^{-1}$  Pa to 20 Pa. For ZnO ETLs of the perovskite solar cell, the optimized oxygen pressure is around 5–10 Pa in terms of both resistivity and transmittance.

## (2) Planar Perovskite Solar Cells with Different ZnO Films as ETLs

Figures 5(a), (c), and (e) illustrate the plan-view images of individual ZnO, perovskite and P3HT layers, respectively. The cross-sectional SEM image of the as-deposited ZnO film is clearly illustrated in Fig. 5(b) and the film thickness is about 70 nm. As shown in Fig. 5(c), the average grain of the spin-coated perovskite layer is found to be ~200 nm,

and the thickness is about 400 nm. It is noteworthy that the precursor materials, e.g., Cl doped-PbI<sub>2</sub> and CH<sub>3</sub>NH<sub>3</sub>I, partially react with each other during the spin coating process, particularly at the interfaces between PbI<sub>2</sub> and CH<sub>3</sub>NH<sub>3</sub>I. The as-prepared CH<sub>3</sub>NH<sub>3</sub>PbI<sub>3</sub> films are initially yellowish-brown in color and subsequently change to dark brown. A small molecule organic polymer P3HT layer can be observed in Fig. 5(e). Figure 5(f) shows the typical cross-sectional SEM image of the planar perovskite solar cell with the following layered structure: FTO/ZnO/perovskite absorber/P3HT/Au.

Figure 6(a) shows the steady-state PL spectrum of intrinsic ZnO film measured at room temperature with a 313 nm excitation light. For intrinsic ZnO sample, a sharp PL peak appears in the UV region centered around 380 nm, which is attributed to a near-band-edge recombination.<sup>38,39</sup> For mixed halide perovskites CH<sub>3</sub>NH<sub>3</sub>PbI<sub>3-x</sub>Cl<sub>x</sub> sample, we adopt 450 nm light from diode laser as the excitation source. It is

noted that the emission peak for the solution-processed  $\text{CH}_3\text{NH}_3\text{PbI}_{3-x}\text{Cl}_x$  film is located at 767 nm with the calculated optical band gap of about 1.61 eV. The glass substrate and  $\text{PbI}_2$  film have no emission peak in this position. Optical absorption spectra were measured on ZnO film, Cl-doped  $\text{PbI}_2$  film and perovskite film, respectively, as shown in Fig. 6(b). The absorption spectrum of the ZnO layer exhibits an absorption edge at 380 nm, which corresponds to its band gap absorption.<sup>9</sup> The adsorption edge of the Cl-doped  $\text{PbI}_2$  locates at about 450 nm. Compared with that of pure  $\text{PbI}_2$

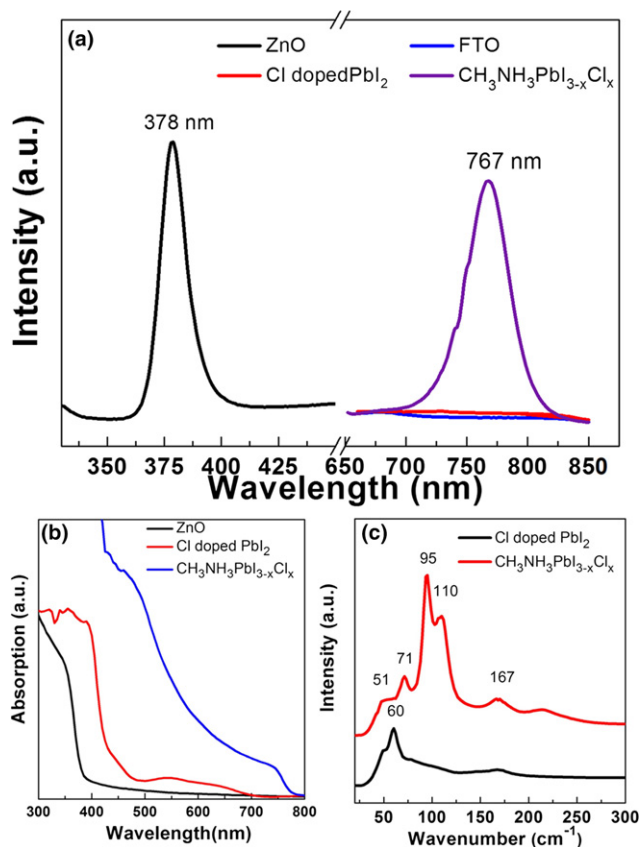


**Fig. 6.** (a) Steady-state PL spectrum of ZnO film and FTO glass, Cl-doped  $\text{PbI}_2$ ,  $\text{CH}_3\text{NH}_3\text{PbI}_{3-x}\text{Cl}_x$  samples excited by 313 and 450 nm light, respectively, (b) UV-vis spectra of ZnO, Cl-doped  $\text{PbI}_2$  film and  $\text{CH}_3\text{NH}_3\text{PbI}_{3-x}\text{Cl}_x$  sample, (c) Raman scattering spectra of ZnO, Cl-doped  $\text{PbI}_2$  film and  $\text{CH}_3\text{NH}_3\text{PbI}_{3-x}\text{Cl}_x$  perovskite absorber under the excitation source of 532 nm.

film (~520 nm),<sup>40</sup> the absorption edge shifts to a higher energy direction. This is mainly because Cl doping widens band gap of  $\text{PbI}_2$  film. The optical absorption onset of the  $\text{CH}_3\text{NH}_3\text{PbI}_{3-x}\text{Cl}_x$  perovskite film occurs at about 770 nm,<sup>41</sup> consistent with the PL data with a Stokes shift.<sup>42</sup> The Raman spectra were further measured under excitation with 532 nm laser for Cl-doped  $\text{PbI}_2$  film and mixed-halide perovskite  $\text{CH}_3\text{NH}_3\text{PbI}_{3-x}\text{Cl}_x$  on ZnO layer. For the Raman spectrum of Cl-doped  $\text{PbI}_2$  film (black line), only one peak at lower frequency of  $60\text{ cm}^{-1}$  assigned to the bending mode of the Pb-I bond is observed.<sup>43</sup> For mixed-halide perovskite  $\text{CH}_3\text{NH}_3\text{PbI}_{3-x}\text{Cl}_x$  film, four perovskite-related peaks are observed, which are in good agreement with the density functional theory calculation.<sup>44</sup> The peaks at 51 and  $71\text{ cm}^{-1}$  are assigned to the inorganic component of  $\text{CH}_3\text{NH}_3\text{PbI}_{3-x}\text{Cl}_x$ . The feature peaks at 110 and  $167\text{ cm}^{-1}$  are assigned to the vibration of the MA cations.<sup>42</sup> However, the bands at  $95\text{ cm}^{-1}$  is attributed to the symmetric stretch  $A_{1g}$  of  $\text{PbI}_2$  crystal,<sup>45,46</sup> which is due to the degradation of  $\text{CH}_3\text{NH}_3\text{PbI}_{3-x}\text{Cl}_x$  film under strong laser illumination.

To investigate the influence of transparent and conductive properties of ZnO films on the photovoltaic performance of according solar cells, the  $J-V$  curves of the ZnO/ $\text{CH}_3\text{NH}_3\text{PbI}_{3-x}\text{Cl}_x$ /P3HT/Au heterojunction cells are measured as shown in Figure 7. The device parameters are summarized in Table II. The device with ZnO film grown at  $10^{-3}$  Pa as ETL exhibits a  $J_{sc} = 5.79\text{ mA/cm}^2$ , a  $V_{oc} = 0.83\text{ V}$ , a FF = 49.68, and a PCE = 2.4%. With the oxygen pressure for ZnO film increasing from  $10^{-3}$  Pa to 5 Pa, all of the device characteristics like  $V_{oc}$ ,  $J_{sc}$ , and PCE improve obviously. The device has  $V_{oc} = 1.04\text{ V}$ ,  $J_{sc} = 12.50\text{ mA/cm}^2$ , FF = 47.96%, and PCE = 6.3% with ZnO film grown at 5 Pa. Further increases in the oxygen pressures of ZnO film from 10 Pa to  $10^2$  Pa result in some deterioration on device performance. The measured  $J-V$  characteristics show close relation to the transparent and conductive properties of ZnO films. With increase of oxygen pressures from  $10^{-3}$  Pa to 5 Pa, the surface of ZnO film become denser and smoother. Also, the crystal quality of ZnO film improves greatly. So, the  $V_{oc}$  and  $J_{sc}$  improve because of reduced photocarriers recombination. The high optical transmittance is beneficial to improve the utilization efficiency of solar radiation and will enhance the solar cell PCE. The FF value is associated with conductive property of ZnO film. When the oxygen pressure varies from  $10^{-1}$  Pa to 5 Pa, FF values are almost similar due to the similar value of resistance observed in Fig. 4. As expected, the ZnO layers obtained at the oxygen pressure of 5 Pa show significant enhancements for both  $V_{oc}$  and  $J_{sc}$  values compared to the  $10^{-3}$  Pa sample. However, when continuing to increase

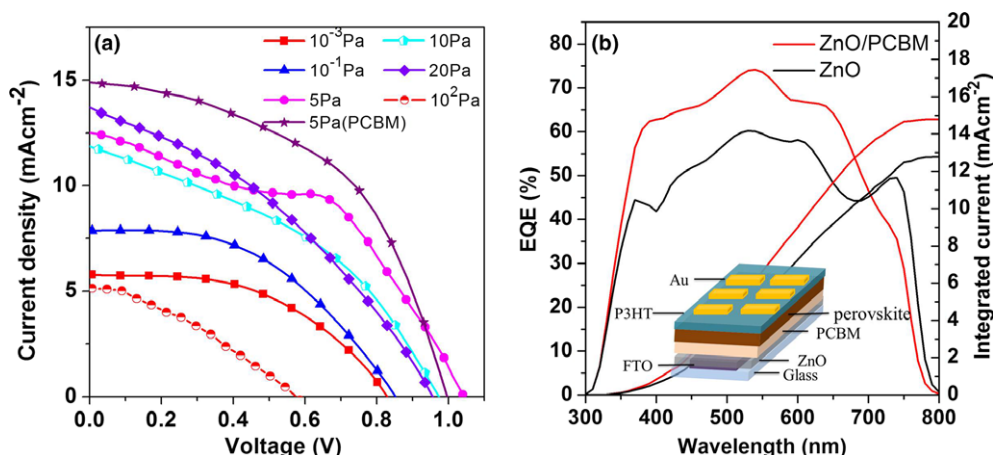


**Fig. 7.** (a) The photocurrent density-voltage ( $J-V$ ) curves of perovskite solar cells based on PLD-ZnO films, (b) external quantum efficiency (EQE) for the best cell using nanostructured ZnO film and ZnO/PCBM, inset is the schematic diagram of the cell device.

**Table II. Photovoltaic Parameters of the PLD-ZnO-Based Perovskite Solar Cells as a Function of Oxygen Pressure**

Buffer layer	$V_{oc}$ (V)	$J_{sc}$ (mA/cm <sup>2</sup> )	FF (%)	PCE (%)
10 <sup>-3</sup> Pa (ZnO)	0.83	5.79	49.68	2.4
10 <sup>-1</sup> Pa (ZnO)	0.85	7.86	47.56	3.2
5 Pa (ZnO)	1.04	12.50	47.96	6.3
5 Pa (ZnO/PCBM)	1.0	14.89	50.21	7.5
10 Pa (ZnO)	0.97	11.86	39.57	4.6
20 Pa (ZnO)	0.97	13.75	36.49	4.9
10 <sup>2</sup> Pa (ZnO)	0.58	5.22	33.29	1.1

oxygen pressures (10 Pa–10<sup>2</sup> Pa), the transparent and conductive properties of ZnO films deteriorate. So, no device performance improvements are observed when the oxygen pressure further increases from 10 Pa to 10<sup>2</sup> Pa.

For a high-efficiency solar cell, except active material itself, device structure and interface are also key factors. In order to modify the interface between ZnO ETL and the perovskite absorber, a PCBM layer is introduced. PCBM is a typical fullerene derivative with good solubility and high electron mobility and has become a standard for organic solar cell electron acceptor. PCBM, as an interface modifier, can combine closely with both the ZnO layer and the absorption layer. Interface modification can help relatively fast extract free electrons and, therefore, enhance the cell performance. After interface modification, the perovskite solar cell exhibits higher characteristic data, e.g.,  $V_{oc} = 1.0$  V,  $J_{sc} = 14.89$  mA/cm<sup>2</sup>, FF = 50.21%, and PCE = 7.5%. Figure 7(b) compares the external quantum efficiency (EQE) spectra from 300 to 800 nm measured from perovskite solar cells with and without PCBM interlayer. With PCBM layer, EQE in almost the whole visible wavelength region is enhanced, thus leading to a clear improvement in  $J_{sc}$ . The integrated photocurrent densities are 14.78 and 12.7 mA/cm<sup>2</sup> corresponding to the solar cells with ZnO and ZnO/PCBM layers, respectively, in good agreement with the experimental results in Table II. The photo-induced free carriers must transfer across the interfaces to be collected, and the charge recombination usually occurs at the interfaces due to interfacial defects.<sup>10</sup> So, introducing a PCBM layer plays an important role in suppressing charge recombination.

#### IV. Conclusion

In summary, we have a detailed research about precisely controlling the semiconductor property of ZnO film like transparency and conductivity that is very important for PSC performance. The photovoltaic performance is explored using a P-i-N solar cell with a ZnO/CH<sub>3</sub>NH<sub>3</sub>PbI<sub>3-x</sub>Cl<sub>x</sub>/P3HT/Au configuration, where PLD grown ZnO film acts as ETL. The best-performing device exhibits a PCE of 6.3% when ZnO ETL is prepared under 5 Pa. When PCBM is further introduced into the solar cell as interface modifier, the PCE was further increased to 7.5%. The high optical transmittance is beneficial to improve the utilization efficiency of solar radiation and the better conductive property of ZnO film is associated with higher FF. So, regulating transparent and conductive properties of ZnO films by controlling the oxygen pressure is essential for developing perovskite solar cells.

#### Acknowledgments

This work is supported by NSFC (51472110, 11174112) and Shandong Provincial Natural Science Foundation (JQ201214, 2014ZRB01A47). The research program from Ministry of Education, China, is also acknowledged (213021A). BC thanks the Taishan Scholar Professorship tenured at University of Jinan and the postgraduate innovation project (YCXB15001) from the University.

#### Supporting Information

Additional Supporting Information may be found in the online version of this article:

**Fig. S1.** SEM images showing the general morphology of ZnO film (a–d). (a) 10<sup>-1</sup> Pa, (b) 5 Pa, (c) 20 Pa, (d) 10<sup>2</sup> Pa.

**Fig. S2.** Full-range of XRD patterns taken from ZnO films under different oxygen pressures. Inset is peak position of ZnO (002) diffraction step scanning of the 2 $\theta$  angle from 33° to 36° (vertical blue line is JCPDS:36-1451, vertical black line of inset is the theoretical (002) angle value for bulk ZnO).

**Fig. S3.** XRD patterns of FTO, Cl-doped PbI<sub>2</sub> and perovskite CH<sub>3</sub>NH<sub>3</sub>PbI<sub>3-x</sub>Cl<sub>x</sub> deposited on a compact ZnO layer on the FTO substrate.

**Table S1.** O 1s analysis of ZnO film synthesized under different oxygen pressures.

#### References

- Y. H. Cheng, Q. D. Yang, J. Y. Xiao, Q. F. Xue, H. W. Li, et al., "Decomposition of Organometal Halide Perovskite Films on Zinc Oxide Nanoparticles," *ACS Appl. Mater. Interfaces*, **7**, 19986–93 (2015).
- H. S. Kim, S. H. Im, and N. G. Park, "Organolead Halide Perovskite: New Horizons in Solar Cell Research," *J. Phys. Chem. C*, **118** [11] 5615–25 (2014).
- H. J. Snaith, "Perovskites: The Emergence of a New Era for Low-Cost, High Efficiency Solar Cells," *J. Phys. Chem. Lett.*, **4**, 3623–30 (2013).
- M. Z. Liu, M. B. Johnston, and H. J. Snaith, "Efficient Planar Heterojunction Perovskite Solar Cells by Vapour Deposition," *Nature*, **501** [19] 395–8 (2013).
- Q. Chen, H. P. Zhou, Z. R. Hong, S. Luo, H. S. Duan, et al., "Planar Heterojunction Perovskite Solar Cells via Vapor-Assisted Solution Process," *J. Am. Chem. Soc.*, **136** [2] 622–5 (2014).
- J. H. Im, I. H. Jang, N. Pellet, M. Graetzel, and N. G. Park, "Growth of CH<sub>3</sub>NH<sub>3</sub>PbI<sub>3</sub> Cuboids with Controlled Size for High-Efficiency Perovskite Solar Cells," *Nat. Nanotechnol.*, **9**, 927–32 (2014).
- W. Nie, H. Tsai, R. Asadpour, J. C. Blancon, A. J. Neukirch, et al., "High-Efficiency Solution-Processed Perovskite Solar Cells with Millimeter-Scale Grains," *Science*, **347**, 522–5 (2015).
- J. H. Heo, H. J. Han, D. Kim, T. K. Ahn, and S. H. Im, "Hysteresisless Inverted CH<sub>3</sub>NH<sub>3</sub>PbI<sub>3</sub> Planar Perovskite Hybrid Solar Cells with 18.1% Power Conversion Efficiency," *Energy Environ. Sci.*, **8**, 1602–8 (2015).
- E. J. Juarez-Perez, M. Wüffler, F. Fabregat-Santiago, K. Lakus-Wollny, E. Mankel, et al., "Role of the Selective Contacts in the Performance of Lead Halide Perovskite Solar Cells," *J. Phys. Chem. Lett.*, **5**, 680–5 (2014).
- J. Shi, X. Xu, D. M. Li, and Q. B. Meng, "Interfaces in Perovskite Solar Cells," *Small*, **11** [21] 2472–86 (2015).
- G. C. Xing, N. Mathews, S. Y. Sun, S. S. Lim, Y. M. Lam, et al., "Long-Range Balanced Electron-and Hole-Transport Lengths in Organic-Inorganic CH<sub>3</sub>NH<sub>3</sub>PbI<sub>3</sub>," *Science*, **342**, 344–7 (2013).
- S. D. Stranks, G. E. Eperon, G. Grancini, C. Menelaou, M. J. P. Alcocer, et al., "Electron-Hole Diffusion Lengths Exceeding 1 Micrometer in an Organometal Trihalide Perovskite Absorber," *Science*, **342**, 341–4 (2013).
- J. Kim, G. Kim, T. K. Kim, S. Kwon, H. Back, et al., "Efficient Planar-Heterojunction Perovskite Solar Cells Achieved via Interfacial Modification of a Sol-Gel ZnO Electron Collection Layer," *J. Mater. Chem. A*, **2**, 17291–6 (2014).
- X. Dong, H. Hu, B. Lin, J. Ding, and N. Yuan, "The Effect of ALD-ZnO Layers on the Formation of CH<sub>3</sub>NH<sub>3</sub>PbI<sub>3</sub> with Different Perovskite Precursors and Sintering Temperatures," *Chem. Commun.*, **50**, 14405–8 (2014).
- D. Q. Bi, W. Tress, M. I. Dar, P. Gao, J. S. Luo, et al., "Efficient Luminescent Solar Cells Based on Tailored Mixed-Cation Perovskites," *Sci. Adv.*, **2** [1] 1501170, 8 pp (2016).
- Q. F. Zhang, C. S. Dandaneau, X. Y. Zhou, and G. Z. Cao, "ZnO Nanostructures for Dye-Sensitized Solar Cells," *Adv. Mater.*, **21**, 4087–108 (2009).
- X. L. Hu, H. B. Gong, H. Y. Xu, H. M. Wei, B. Q. Cao, et al., "Influences of Target and Liquid Media on Morphologies and Optical Properties of ZnO Nanoparticles Prepared by Laser Ablation in Solution," *J. Am. Chem. Soc.*, **94** [12] 4305–9 (2011).
- H. Li, Y. Zhang, and J. Wang, "ZnO Nanosheets Derived From Surfactant-Directed Process: Growth Mechanism, and Application in Dye-Sensitized Solar Cells," *J. Am. Chem. Soc.*, **95** [4] 1241–6 (2012).
- D. Liu, M. K. Gangishetty, and T. L. Kelly, "Effect of CH<sub>3</sub>NH<sub>3</sub>PbI<sub>3</sub> Thickness on Device Efficiency in Planar Heterojunction Perovskite Solar Cells," *J. Mater. Chem. A*, **2**, 19873–81 (2014).
- D. Liu, J. Yang, and T. L. Kelly, "Compact Layer Free Perovskite Solar Cells with 13.5% Efficiency," *J. Am. Chem. Soc.*, **136** [49] 17116–22 (2014).
- D. Y. Son, J. H. Im, H. S. Kim, and N. G. Park, "11% Efficient Perovskite Solar Cell Based on ZnO Nanorods: An Effective Charge Collection System," *J. Phys. Chem. C*, **118**, 16567–73 (2014).

- <sup>22</sup>D. Liu and T. L. Kelly, "Perovskite Solar Cells with a Planar Heterojunction Structure Prepared Using Room-Temperature Solution Processing Techniques," *Nature Photon*, **8**, 133–8 (2014).
- <sup>23</sup>K. Mahmood, B. S. Swain, and A. Amassian, "Double-Layered ZnO Nanostructures for Efficient Perovskite Solar Cells," *Nanoscale*, **6**, 14674–8 (2014).
- <sup>24</sup>J. X. Song, J. Bian, E. Q. Zheng, X. F. Wang, W. J. Tian, and T. Miyasaka, "Efficient and Environmentally Stable Perovskite Solar Cells Based on ZnO Electron Collection Layer," *Chem. Lett.*, **44**, 610–2 (2015).
- <sup>25</sup>Z. L. Tseng, C. H. Chiang, and C. G. Wu, "Surface Engineering of ZnO Thin Film for High Efficiency Planar Perovskite Solar Cells," *Sci. Rep.*, **5**, 13211–20 (2015).
- <sup>26</sup>Z. W. Liu and C. K. Ong, "Synthesis and Size Control of ZnO Nanorods by Conventional Pulsed-Laser Deposition Without Catalysis," *Mater. Lett.*, **61** [16] 3329–33 (2007).
- <sup>27</sup>S. S. Lin, J. I. Hong, J. H. Song, Y. Zhu, H. P. He, et al., "Phosphorus Doped Zn<sub>1-x</sub>Mg<sub>x</sub>O Nanowire Arrays," *Nano Lett.*, **9** [11] 3877–82 (2009).
- <sup>28</sup>B. Q. Cao, J. Z. Pérez, C. Czekalla, H. Hilmer, J. Lenzner, et al., "Tuning the Lateral Density of ZnO Nanowire Arrays and Its Application as Physical Templates for Radial Nanowire Heterostructures," *J. Mater. Chem.*, **20**, 3848–54 (2010).
- <sup>29</sup>P. F. Carcia, R. S. McLean, M. H. Reilly, and G. Nunes, "Transparent ZnO Thin-Film Transistor Fabricated by rf Magnetron Sputtering," *Appl. Phys. Lett.*, **82**, 1117–9 (2003).
- <sup>30</sup>A. Hausmann and B. Utsch, "Oxygen Ion Vacancies as Donors in Zinc-Oxide," *Zeitschrift für Physik B-Condensed Matter*, **21** [3] 217–20 (1975).
- <sup>31</sup>J. Das, S. K. Pradhan, D. R. Sahu, D. K. Mishra, S. N. Sarangi, et al., "Micro-Raman and XPS Studies of Pure ZnO Ceramics," *Phys. B*, **405**, 2492–7 (2010).
- <sup>32</sup>C. D. Wagner, L. H. Gale, and R. H. Raymond, "Two-Dimensional Chemical State Plots: A Standardized Data Set for Use in Identifying Chemical States by X-ray Photoelectron Spectroscopy," *Anal. Chem.*, **51**, 466–82 (1979).
- <sup>33</sup>Y. Du, M. S. Zhang, J. Hong, Y. Shen, Q. Chen, and Z. Yin, "Structural and Optical Properties of Nanophase Zinc Oxide," *Appl. Phys. A*, **76**, 171–6 (2003).
- <sup>34</sup>B. Q. Cao, W. P. Cai, and H. B. Zeng, "Temperature-Dependent Shifts of Three Emission Bands for ZnO Nanoneedle Arrays," *Appl. Phys. Lett.*, **88**, 161101–3 (2006).
- <sup>35</sup>C. F. Klingshim, B. K. Meyer, A. Waag, A. Hoffmann, and J. Geurts, *Zinc Oxide: From Fundamental Properties Towards Novel Applications*, 104–5. Springer, New York City, New York, 2010.
- <sup>36</sup>J. Dong, Y. Zhao, J. Shi, H. Wei, J. Xiao, et al., "Impressive Enhancement in the Cell Performance of ZnO Nanorod-Based Perovskite Solar Cells with Al Doped ZnO Interfacial Modification," *Chem. Commun.*, **50**, 13381–4 (2014).
- <sup>37</sup>D. H. Kim, N. G. Cho, H. G. Kim, and W. Y. Choi, "Structural and Electrical Properties of Indium Doped ZnO Thin Films Fabricated by RF Magnetron Sputtering," *J. Electrochem. Soc.*, **154** [11] 939–43 (2007).
- <sup>38</sup>Z. W. Qiu, X. P. Yang, J. Han, P. Zhang, B. Q. Cao, et al., "Sodium-Doped ZnO Nanowires Grown by High-Pressure PLD and Their Acceptor-Related Optical Properties," *J. Am. Chem. Soc.*, **97** [7] 2177–84 (2014).
- <sup>39</sup>D. A. Guzmán-Embús, M. F. Vargas-Charry, and C. Vargas-Hernández, "Optical and Structural Properties of ZnO and ZnO:Cd Particles Grown by the Hydrothermal Method," *J. Am. Chem. Soc.*, **98** [5] 1498–505 (2015).
- <sup>40</sup>M. M. Lee, J. Teuscher, T. Miyasaka, T. N. Murakami, and H. J. Snaith, "Efficient Hybrid Solar Cells Based on Meso-Superstructured Organometal Halide Perovskites," *Science*, **338**, 643–7 (2012).
- <sup>41</sup>P. Qin, N. Tetreault, M. I. Dar, P. Gao, K. L. McCall, et al., "A Novel Oligomer as a Hole Transporting Material for Efficient Perovskite Solar Cells," *Adv. Energy Mater.*, **5** [2] 1400980–4 (2014).
- <sup>42</sup>C. Quarti, G. Grancini, E. Mosconi, P. Bruno, J. M. Ball, et al., "The Raman Spectrum of the CH<sub>3</sub>NH<sub>3</sub>PbI<sub>3</sub> Hybrid Perovskite: Interplay of Theory and Experiment," *J. Phys. Chem. Lett.*, **5**, 279–84 (2014).
- <sup>43</sup>N. Preda, L. Mihut, M. Baibarac, M. Husanu, C. Bucur, and I. Baltog, "Raman and Photoluminescence Studies on Intercalated Lead Iodide with Pyridine and Iodine," *J. Optoelectron. Adv. Mater.*, **10**, 319–22 (2008).
- <sup>44</sup>B. W. Park, S. M. Jain, X. L. Zhang, A. Hagfeldt, G. Boschloo, and T. Edvinsson, "Resonance Raman and Excitation Energy Dependent Charge Transfer Mechanism in Halide-Substituted Hybrid Perovskite Solar Cells," *ACS Nano*, **9** [2] 2088–101 (2015).
- <sup>45</sup>S. Nakashima, "Raman Study of Polytypism in Vapor-Grown PbI<sub>2</sub>," *Solid State Commun.*, **16**, 1059–62 (1975).
- <sup>46</sup>V. Capozzi, A. Fontana, M. Fontana, G. Mariotto, M. Montagna, and G. Viliani, "Raman-Scattering in PbI<sub>2</sub>," *Il Nuovo Cimento B*, **39**, 556–68 (1977). □